The Changing Shape of the Ionosphere During a Solar Eclipse

Tobias G. W. Verhulst and Stanimir M. Stankov

Abstract – Solar eclipses affect not only the ionospheric layers' peak densities and heights but also the general shape of the electron density profile. We revisit data obtained from the ionosonde in Dourbes, Belgium, during the solar eclipse of March 20, 2015. Previously, these observations were used to study the behavior of the F and E layer peaks and the plasma drifts. We investigate here which shape parameters of the bottom-side ionosphere were affected during this event. We find that the International Reference Ionosphere parameter B_0 is most affected, while B_1 is not affected by the eclipse at all. The scale height and slab thickness also show some effects but less so than B_0.

1. Introduction

It has been known for some time that observations of the ionosphere during a solar eclipse can be used as a method for studying various aspects of the ionosphere [1–3]. In recent decades, modern ionosondes have been used for such observations at relatively small time resolution during various eclipses; see, for example, [4–8].

In different studies, particular aspects of the ionosphere have been investigated: [4] and [6] focused on wave-like disturbances, [5] presented observations of plasma drift together with the effects on different International Union of Radio Science (URSI) parameters (f_oE, f_oF_2, and hmF_2), and [7] used NmF_2 data derived from ionograms to validate physics-based modeling work.

As already described in [1, 9], the quick movement of the lunar shadow results in a non-equilibrium condition in the ionosphere. In addition, the altitude dependency of the obscuration during an eclipse [10] and the effects of the non-uniformity of the solar disk in the EUV spectrum [7, 11] have to be taken into account. Thus, it can be expected that not only the characteristics of the peaks of the ionospheric layers will be affected by a solar eclipse but also the entire shape of the electron density profile. Some indications of this can be observed in the empirical data presented in [5] and [8], and it is evident in the model results shown in [7, fig. 11]. In both cases, it can be seen that the ionosphere at different altitudes reacts with different delays and timescales to the eclipse, leading to deviations from the normal shape of the electron density profile.

Here, we will investigate the behavior of some empirical parameters used for describing the shape of the bottom-side electron density profile during the solar eclipse of 20 March, 2015.

Manuscript received 23 December 2022.

Tobias G. W. Verhulst and Stanimir M. Stankov are with the Solar Terrestrial Center of Excellence, Royal Meteorological Institute, Ringlaan 3, Brussels, Belgium; e-mail: tobias.verhulst@oma.be.

2. Data

We examine the observations obtained by the Digisonde-4D ionosonde installed in Dourbes, Belgium (URSI code: DB049). The observatory is located at 50.1°N, 4.6°E, and experienced a maximal obscuration at ground level of 78.1%. The eclipse started at 08:26 UT and ended at 10:45 UT, with the maximal obscuration at 09:34 UT (all times given for ground level).

During the time of the eclipse, as well as on the following day at the same time, a campaign of high time resolution soundings was performed. This campaign is described in detail in [5], where the behavior of the F_2 and E peaks and of the plasma drift were investigated. Here, we reanalyze the same ionograms, investigating instead various parameters related to the shape of the bottom-side electron density profile. Observations obtained on the day after the eclipse, which was not disturbed by geomagnetic activity (there was a major disturbance on March 16 and 17, with *Dst* dropping to –234 nT), are used for comparison. All ionograms, scaled characteristics, and reconstructed electron density profiles are freely available through the Global Ionospheric Radio Observatory repository [12].

We rely on characteristics automatically scaled by the Automatic Real-Time Ionogram Scaler with True height (ARTIST-5) software and electron density profiles reconstructed by the NHPC method [13]. As discussed in [5], the automatically scaled parameters and consequentially the reconstructed electron density profiles obtained during the campaign were generally quite reliable. Nevertheless, some clearly erroneous outliers can be seen in the figures below, representing cases of faulty scaling of the ionograms. These cases are not so numerous as to present a problem for our analyses.

We include here four different parameters characterizing the shape of the bottom-side F_2 layer. First, we look at the bottom-side scale height H_{SC} and the parabolic layer semi-thickness y_{F_2}. Both these parameters provide an indication of the slab thickness of the F_2 layer. Unless there is a major problem with the scaling of the ionogram, they are expected to exhibit similar behavior. We include both parameters for the purpose of cross-validation. In addition, we include two

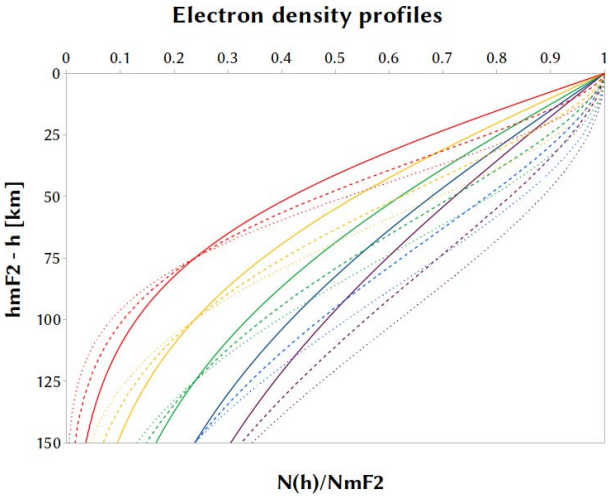

Figure 1. Bottom-side electron density profiles for different values of B_0 and B_1. The density is given relative to the peak density and the height in kilometers below the peak. B_0 is taken equal to 75 km (red), 100 km (yellow), 125 km (green), 150 km (blue), and 175 km (purple). Solid, dashed, and dotted lines correspond, respectively, to B_1 values of 1.0, 1.5, and 2.0.

parameters used by the International Reference Ionosphere (IRI) model to describe the shape of the F_2 layer: B_0 and B_1. These parameters are defined by describing the electron density $N(h)$ in function of the height in the bottom-side F_2 layer using a modified Epstein profile (see [14, 15] and the references therein):

$$N(h) = NmF_2 \frac{e^{-\left(\frac{hmF_2-h}{B_0}\right)^{B_1}}}{\cosh\frac{hmF_2-h}{B_0}} \quad (1)$$

Here, hmF_2 is the height of the F_2 peak, and NmF_2 is the peak electron density. B_0 in (1) is again a thickness parameter and is given in kilometers, while B_1 is a dimensionless exponent describing additional deviation of the profile from the standard Epstein function. Figure 1 shows the shape of the profile for different values of B_0 and B_1. We use the values for B_0 and B_1 best describing the reconstructed electron density distribution.

Empirical relations between B_0 and B_1 as well as between these parameters and the peak characteristics have been established [15, 16]. During the disturbances associated with a solar eclipse, deviations from such climatological relations should be expected because of the above-mentioned non-equilibrium conditions, plasma movement, and so on.

3. Observations

Figure 2 shows the scale height and Figure 3 the semi-thickness of the F_2 layer. In each case, the upper panel displays the data from the day of the eclipse and the lower panel from the day after. For both days, the period from 06:30 to 11:30 UT is shown. The red lines

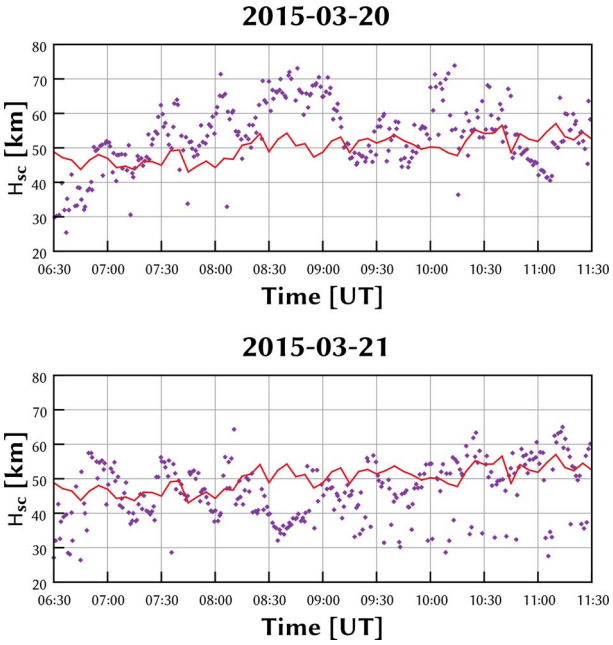

Figure 2. Bottom-side scale height on the day of the eclipse (top panel) and the day after (bottom panel). The solid line presents 28 day median values taken over two 14 day intervals before and after these two days.

show the median values taken over 14 days before and 14 days after the two days under investigation.

It is evident from Figures 2 and 3 that H_{SC} and y_{F_2} generally behave according to similar patterns both on the day of the eclipse and on the succeeding day. It can

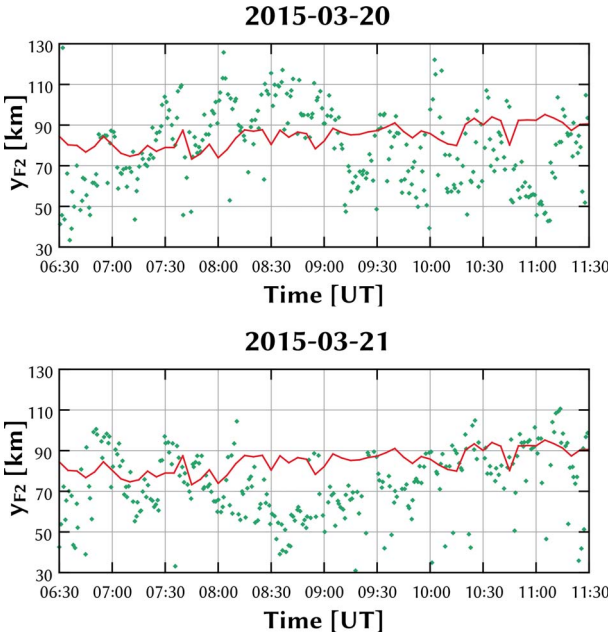

Figure 3. Bottom side slab thickness y_{F_2} of the F_2 layer. The top panel shows the day of the eclipse, the bottom panel the reference day, and the red line the 28 day median.

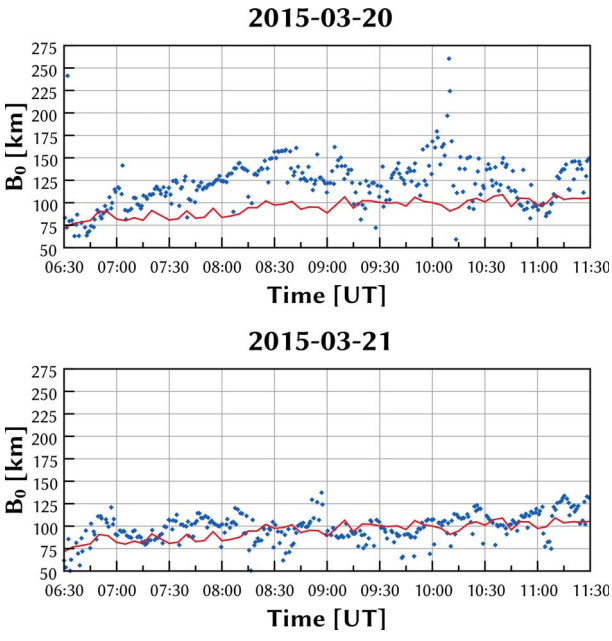

Figure 4. IRI thickness parameter B_0 for the same periods as included in Figures 2 and 3; the red line indicates the long median.

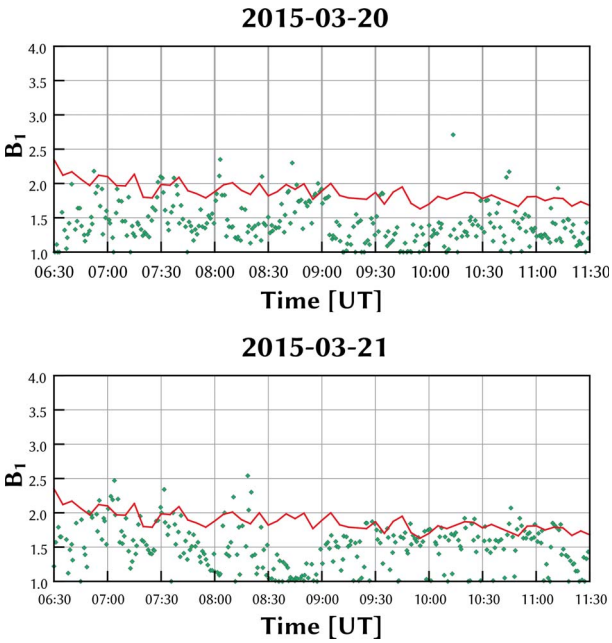

Figure 5. IRI parameter B_1, in dimensionless units, corresponding to the B_0 values shown in Figure 4. The solid line shows the 28 day median.

also be seen that there is significant variability in both these parameters on either day, even when discounting obvious outliers that are likely due to erroneous automatic scaling of the ionograms.

On the day of the eclipse, both parameters show two increases peaking at 07:30 and 08:00 UT, followed by a larger and longer-lasting increase between 08:10 and 09:15, peaking at around 08:45. The latter period corresponds to the onset of the eclipse, when the electron density distribution can be assumed not to be in an equilibrium state and when significant plasma drifts were observed [5, 8]. The earlier peaks are seen before the onset of the event at the height of the F_2 layer. Nevertheless, they coincide with deviations in the peak characteristics [5, 8] and are most likely associated with traveling ionospheric disturbances propagating out from regions covered earlier by the lunar shadow.

Figures 4 and 5 show, respectively, the IRI parameters B_0 and B_1. The periods of observations shown and the median included for reference cover the same time intervals shown in Figures 2 and 3. Again the solid red lines show the 28 day medians.

The B_0 parameter can be seen to be very different on both days. During the day of the eclipse, shown in the upper panel of Figure 4, there is a gradual increase of B_0 starting around the time of the onset of obscuration, followed by a brief return to the median around the maximum of the eclipse, and finally a second increase when the obscuration is decreasing. Note that the vertical axes in Figure 4 cover a wide range in order to include all points. However, the few cases for which B_0 reaches 200 km or higher should not be trusted as accurate. If B_0 reaches such values, it is likely no longer correct to describe the layer using formula (1). The variations up to about 150 km do seem reliable because these values are reached by a gradual change over multiple ionograms and thus cannot be the result of faulty scaling. This represents an increase of almost 100% above the median.

The time of the main increase in B_0, from around 08:00 UT until around 09:15 UT, coincides with the peak seen in H_{SC} and y_{F_2}, and the second peak around 10:00 UT can also be detected in all three parameters. On the other hand, the shorter peaks at earlier times are clearly identifiable in B_0.

On March 21, as can be seen in the lower panel of Figure 4, the B_0 parameter also exhibited some variability but of a smaller amplitude. Also, the observed B_0 values fluctuate above and below the median, while on the eclipse day, B_0 was generally above the median throughout the considered time interval.

Both panels of Figure 5 are similar, with no clear influence of the eclipse visible. It seems therefore that B_1 remains unaffected by the solar eclipse. Interestingly, the values of B_1 on both days are almost all below the median. The other three parameters show some systematic increase on the day of the eclipse—particularly evident for B_0 in Figure 4. But on the day after the eclipse, only B_1 shows a systematic deviation, while the other parameters vary around the median.

4. Discussion and Conclusions

Various parameters are used to describe different aspects of the shape of the electron density profile in the bottom-side ionosphere in different contexts. H_{SC}, y_{F_2},

and B_0 are all measures relating to the thickness of the F_2 layer. In the data presented here, H_{SC} and y_{F_2} are seen to be highly correlated, while B_0 exhibits slightly different variations.

Apparently, the B_0 parameter was the one most clearly affected by the solar eclipse. The relative deviations from the mean during the eclipse reached almost 100%. The scale height and semi-thickness, however, showed evidence of the traveling disturbances arriving above the ionosonde location before the local onset of the eclipse, described in previous analyses of this event [5, 8]. These wave-like disturbances were not detected in B_0. Thus, despite the various thickness parameters in principle being related to each other, it is clear that they all need to be considered in order to observe all aspects of the ionosphere's reaction to a solar eclipse.

No evidence was found for B_1 to be particularly influenced by the eclipse. Variations on both the day of the event and the day after are similar and small. However, it was observed that B_1 during both days fell systematically below the median calculated over 28 days.

This systematic deviation of B_1 from the long-term median, also during the day that is not affected by the solar eclipse, might be a consequence of the major geomagnetic storm on March 16 and 17. The ionosphere was still in the end of the recovery phase of this storm, with *Dst* values gradually increasing from –75 nT to –40 nT over the course of March 20 and 21. For the other parameters, it is unlikely that the observed behavior is due to this geomagnetic disturbance because the differences between the two consecutive days are far larger than those for B_1 (which are essentially non-existent).

One limitation of the results presented here is that only data from a single observatory and for a single eclipse are included. Nevertheless, it is evident that not only the peak characteristics are affected by a solar eclipse. In future work, the different shape parameters of the ionosphere should be analyzed for other events as well.

5. References

1. H. Rishbeth, "Solar Eclipses and Ionospheric Theory," *Space Science Reviews*, **8**, September 1968, pp. 543-554, doi: 10.1007/bf00175006.
2. M. Anastassiades, *Solar Eclipses and the Ionosphere*, New York, Plenum Press, 1970.
3. H. Rishbeth, "Eclipse Effects in the Ionosphere," *Nature*, **226**, June 1970, pp. 1099-1100, doi: 10.1038/2261099a0.
4. D. Altadill, J. G. Solé, and E. M. Apostolov, "Vertical Structure of a Gravity Wave Like Oscillation in the Ionosphere Generated by the Solar Eclipse of August 11, 1999," *Journal of Geophysical Research: Space Physics*, **106**, October 2001, pp. 21419-21428, doi: 10.1029/2001ja900069.
5. T. G. W. Verhulst, D. Sapundjiev, and S. M. Stankov, "High-Resolution Ionospheric Observations and Modeling Over Belgium During the Solar Eclipse of 20 March 2015 Including First Results of Ionospheric Tilt and Plasma Drift Measurements," *Advances in Space Research*, **57**, March 2016, pp. 2407-2419, doi: 10.1016/j.asr.2016.03.009.
6. T. G. W. Verhulst and S. M. Stankov, "Ionospheric Wave Signature of the American Solar Eclipse on 21 August 2017 in Europe," *Advances in Space Research*, **61**, February 2018, pp. 1797-1806, doi: 10.1016/j.asr.2017.05.042.
7. S. Mrak, Q. Zhu, Y. Deng, I. E. Dammasch, M. Dominique, M. R. Hairston, Y. Nishimura, and J. Semeter, "Modeling Solar Eclipses at Extreme Ultra Violet Wavelengths and the Effects of Nonuniform Eclipse Shadow on the Ionosphere-Thermosphere System," *Journal of Geophysical Research: Space Physics*, **127**, December 2022, e2022JA031058, doi: 10.1029/2022ja031058.
8. S. M. Stankov, N. Bergeot, D. Berghmans, D. Bolsée, C. Bruyninx, J.-M. Chevalier, F. Clette, H. De Backer, J. De Keyser, E. D'Huys, M. Dominique, J. F. Lemaire, J. Magdalenić, C. Marqué, N. Pereira, V. Pierrard, D. Sapundjiev, D. B. Seaton, K. Stegen, R. Van der Linden, T. G. W. Verhulst, and M. J. West, "Multi-Instrument Observations of the Solar Eclipse on 20 March 2015 and Its Effects on the Ionosphere Over Belgium and Europe," *Journal of Space Weather and Space Climate*, **7**, 2017, A19, doi: 10.1051/swsc/2017017.
9. B. H. Briggs and H. Rishbeth, "An Analogue Solution of the Continuity Equation of the Ionospheric F Region," *Proceedings of the Physical Society*, **78**, September 1961, pp. 409-422, doi: 10.1088/0370-1328/78/3/310.
10. T. G. W. Verhulst and S. M. Stankov, "Height Dependency of Solar Eclipse Effects: The Ionospheric Perspective," *Journal of Geophysical Research: Space Physics*, **125**, June 2020, e2020JA028088, doi: 10.1029/2020JA028088.
11. S. Mrak, J. Semeter, D. Drob, and J.D. Huba, "Direct EUV/X-Ray Modulation of the Ionosphere During the August 2017 Total Solar Eclipse," *Geophysical Research Letters*, **45**, May 2018, pp. 3820-3828, doi: 10.1029/2017GL076771.
12. B. W. Reinisch and I. A. Galkin, "Global Ionospheric Radio Observatory (GIRO)," *Earth, Planets, and Space*, **63**, April 2011, pp. 377-381, doi:10.5047/eps.2011.03.001.
13. X. Huang and B. Reinisch, "Vertical Electron Density Profiles From the Digisonde Network," *Advances in Space Research*, **18**, January 1996, pp. 121-129, doi: 10.1016/0273-1177(95)00912-4.
14. D. Bilitza, *International Reference Ionosphere 1990*, NSSDC/WDC-A-R&S 90-22, 1990.
15. D. Bilitza and K. Rawer, "New Options for IRI Electron Density in the Middle Ionosphere," *Advances in Space Research*, **10**, 11, 1990, pp. 7-16, doi: 10.1016/0273-1177(90)90299-f.
16. T. Gulyaeva, "Progress in Ionospheric Informatics Based on Electron-Density Profile Analysis of Ionograms," *Advances in Space Research*, **7**, 6, 1987, pp. 39-48, doi: 10.1016/0273-1177(87)90269-9.